APL MATERIALS **1**, 062107 (2013)

La-doped $BaTiO_3$ heterostructures: Compensating the polarization discontinuity

D. P. Kumah,[1,a] Y. Yacoby,[2] S. A. Pauli,[3] P. R. Willmott,[3] and R. Clarke[1,b]
[1]*Applied Physics Program, University of Michigan, Ann Arbor, Michigan 48109, USA*
[2]*Racah Institute of Physics, Hebrew University, Jerusalem 91904, Israel*
[3]*Swiss Light Source, Paul Scherrer Institut, CH-5232 Villigen PSI, Switzerland*

(Received 20 September 2013; accepted 4 December 2013; published online 18 December 2013)

We demonstrate a route to manipulate the polarization and internal electric field of a complex oxide heterostructure using a layering sequence based on the $LaAlO_3$-$SrTiO_3$ interface. By combining sensitive atomic-level mapping of the structure using direct x-ray phase-retrieval methods with theoretical modeling of the electrostatic charge and polarization, we have devised a novel single-domain polar heterostructure. We find that ionic rearrangement results in strain and free energy minimization, and eliminates the polarization discontinuity leading to a two-fold increase of the spontaneous polarization towards the surface of an ultra-thin single-domain $BaTiO_3$ film. [http://dx.doi.org/10.1063/1.4849735]

Atomic-scale structural, chemical, and electronic interactions at interfaces in complex-oxide heterostructures hold the key to a fascinating array of correlated-electron phenomena, including novel superconducting phases, colossal magnetoresistance, multiferroicity, and 2D electron-gas behavior.[1–3] These effects arise from a subtle interplay of ionic and electronic rearrangements in response to interfacial boundary conditions which often give rise to new properties that are not found in the parent bulk materials. One of the most interesting interfacial phenomena in complex oxides is the appearance of a highly conducting interface between appropriately terminated epitaxial $LaAlO_3$ (LAO) and $SrTiO_3$ (STO) layers.[3] In this case, it is known that a polar reconstruction above a critical thickness of ∼3.5 monolayers leads to injection of electrons across the interface to produce trivalent titanium ions with itinerant 3*d* electrons, providing the 2D conductivity.[3–6] This provides an elegant mechanism to mitigate the so-called polar catastrophe.

In this letter, we explore whether a similar electronic reconstruction can occur at the interface between a ferroelectric, $BaTiO_3$(BTO), and a monolayer of a Mott insulator, $LaTiO_3$. The formation of a highly conducting two-dimensional electron gas at the nominally polar insulator/BTO interface could be useful for mitigating the polarization discontinuities in ferroelectric heterostructures. In such materials it is well known that depolarization fields can cancel the spontaneous polarization of thin ferroelectric films (e.g., BTO on STO),[7] thereby rendering them ineffective for applications in sensors, non-volatile memory devices, and transducers.[8] While we do indeed achieve single-domain polarization in the nominal BTO films, it differs from what we originally anticipated: what actually happens is that La diffuses from the LTO layer. As we will show, the uniform doping of La in BTO leads to a linear polarization profile, rising from zero at the lower surface of the BTO to a substantially enhanced value at its uppermost surface.

The heterostructures were grown using pulsed laser deposition on TiO_2-terminated STO substrates. A schematic of the heterostructure is shown in Fig. 1(a). Note that the detailed growth

[a]Present address: Center for Research on Interface Structures and Phenomena, Yale University, New Haven, Connecticut 06511, USA.
[b]Electronic mail: royc@umich.edu

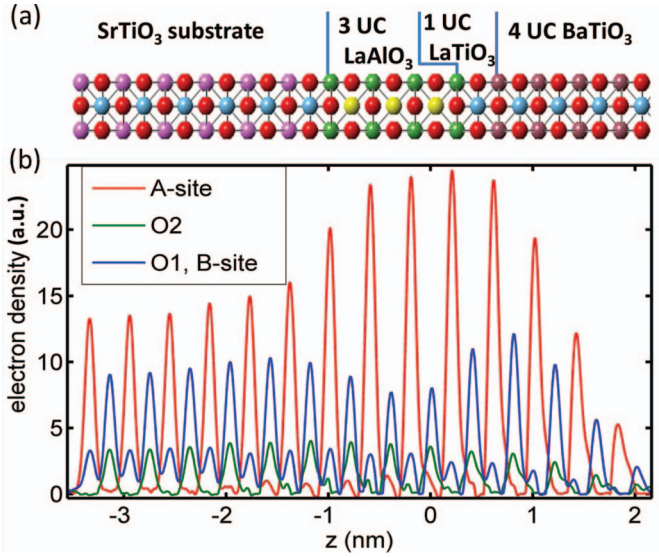

FIG. 1. (a) Schematic of nominal STO/LAO/LTO/BTO heterostructure and (b) electron-density profile measured using the COBRA x-ray phase-retrieval method. The approximate nominal LAO/LTO interface is at z = 0 nm. UC refers to the perovskite unit cell.

sequence includes a single unit cell of $LaTiO_3$ (LTO) inserted between the LAO and BTO in order to mimic the ionic reconstruction previously found to occur at the STO-LAO interface.[9] The laser fluence was 1 J cm^{-2}, and the O_2 base pressure was 5×10^{-5} mbar, and the substrate temperature was 730 ± 20 °C. Post-growth annealing was performed at 550 °C for 1 h in O_2 at atmospheric pressure. Two samples were prepared: one with a surface electrode consisting of 10 nm of polycrystalline Au, and a second one without the Au coating. The conductivity of the STO-LAO interface was measured in the latter sample and found to be insulating.

To determine the atomic structure and polarization of the heterostructures, x-ray diffraction intensities along crystal truncation rods (CTRs) were measured at the X04 beam line of the Swiss Light Source with an incident x-ray energy of 16 keV. The samples were mounted in an evacuated Be-domed chamber to prevent radiation damage during the measurements. Ten symmetry-inequivalent rods were measured.

The CTRs were converted to real space three-dimensional (3D) electron density maps using the Coherent Bragg Rod Analysis (COBRA) technique.[10–12] The atomic structure of the film layers was determined from the 3D maps with sub-Ångstrom resolution (see supplementary material for further information).[13] Scattering from the polycrystalline Au top electrode does not contribute to the measured CTRs, hence, the structural analysis of the oxide heterostructure is not affected by the Au. From the electron-density maps, the layer-resolved lattice spacing, chemical composition, and polar distortions were derived. Figure 1(b) shows the vertical line profiles through the inequivalent atomic positions in the perovskite structure. The integrated intensities of the electron density peaks are proportional to the atomic scattering factors of the atoms occupying the respective crystallographic sites. The layer-resolved chemical profile and atomic positions are determined from fits to the Gaussian-like peaks.

Figure 2 shows the measured layer-resolved fractional composition profile as a function of ionic positions for the nominal epitaxial heterostructure composed of: STO substrate/3 UC LAO/1 UC LTO/4 UC BTO, where UC refers to a unit cell of the bulk perovskite structure. For the A-site profile, a gradual transition is observed from Sr to La across the STO/LAO interface indicative of a Sr-La ionic rearrangement at the STO/LAO interface as previously observed.[9] A similar transition is observed along the B-site (Ti,Al) profile indicative of Ti/Al intermixing across the STO/LAO interface. The transition from La to Ba at the LTO/BTO interface is indistinguishable from the A-site profile, within our experimental sensitivity, because La and Ba have similar scattering factors at

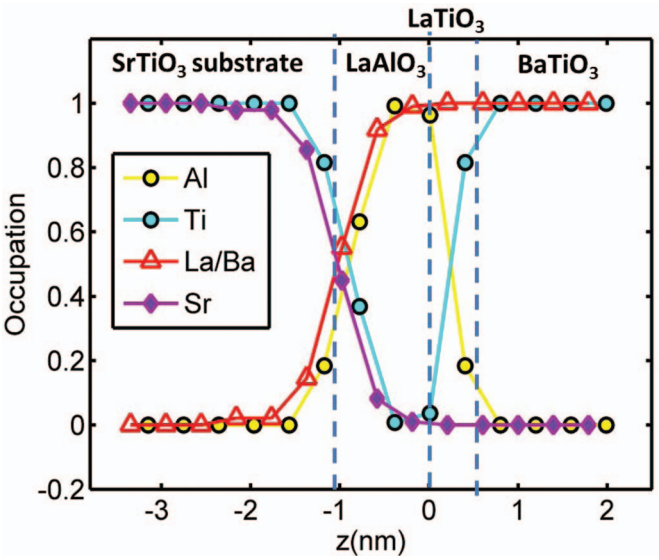

FIG. 2. Layer-resolved composition distribution for a nominally STO substrate/3UC LAO/1 UC LTO/4UC BTO sample, derived from the COBRA-determined electron-density map in Fig. 1(b). The dashed lines indicate the nominal interfaces; z = 0 corresponds approximately to the lower surface of the nominal LTO layer.

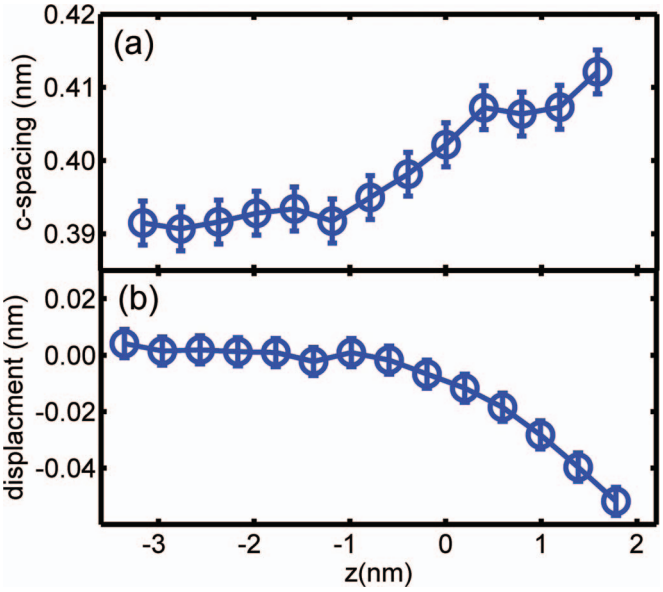

FIG. 3. (a) Layer-resolved lattice spacings, and (b) vertical displacements, in the AO layers between the oxygen anions and the A-site cations (Sr,La,Ba) of the heterostructure. z = 0 corresponds approximately to the lower surface of the nominal LTO layer. Negative displacements are towards the substrate.

16 keV (57 for Ba and 58 for La). However, it will be shown below that La uniformly dopes the BTO layer.

The layer-resolved spacings between the A-site layers are shown in Fig. 3(a). The layer spacing in the STO substrate region ($z < -1$ nm) is 0.3905 nm, as expected for bulk STO. A gradual expansion of the lattice spacing occurs in the nominal LAO region (-1 nm $< z < 0$ nm) to 0.4074 nm where the nominal BTO layer begins.

The expected out-of-plane spacing of the nominal BTO strained to the STO substrate is 0.412 nm. The observed slightly reduced lattice spacing in the nominal BTO region of 0.4074 nm is consistent with La redistribution into the BTO film.[14] The substitutional doping of Ba^{2+} (ionic

TABLE I. Parameters used to model the BTO:La component of the ferroelectric heterostructure.

Parameter	Symbol	Value	Ref.
Number of La ions per unit area	N_1	6.56×10^{18} m^{-2}	
Relative optical dielectric constant[a]	ϵ_∞	5.7	17
Spontaneous polarization[a]	P_S	0.25 C/m^2	18
	α	-2.0×10^8 J m/C^2	19
	β	-18.7×10^8 J m^5/C^4	19
	γ	8.2×10^{10} J m^9/C^6	19
	g	4.2×10^{-10} J m^3/C^2	

[a]Bulk.

radius = 0.160 nm) with La^{3+} (ionic radius = 0.136 nm) effectively reduces the strain energy, and as will be discussed later in this paper, leads to a gradual increase in the electrical polarization. Note that Ba^{2+} will not replace La^{3+} in LAO because of valence mismatch. The alloyed LTO/BTO region will, henceforth, be referred to as BLTO.

The electron-density maps enable us to measure, with great precision, the relative vertical displacement between the O anions and A-site cations in the AO atomic planes. The measured polar displacements are shown in Fig. 3(b) as a function of layer. Within the experimental uncertainties, no polar displacements are observed in the STO substrate nor in the nominally LAO layer. However, in the BLTO region, the O anions are displaced relative to the Ba cations towards the STO substrate. The amplitude of the displacement increases approximately linearly from the BLTO/LAO interface to the BLTO surface. At the surface, the oxygen displacements are about 2 times larger than typical displacements of the oxygen relative to the cations in bulk BTO.[16] Analysis of a similar sample with no top Au electrode gave the same results.

The oxygen displacement relative to the Ba atoms shown in Fig. 3(b) means that essentially all apical oxygen ions in a macroscopic area are displaced in the same direction, namely, towards the substrate, forming a polar single-domain state. We do not observe diffuse scattering related to multi-domains.[11] Theoretical considerations as well as experimental measurements[15] have shown that due to strong depolarizing electric fields, neither multidomain nor single ferroelectric domains will form in a BTO film confined between two insulators (i.e., the BTO remains unpolarized). In the present experiment we find that the presence of surface charge and the migration of La^{3+} into the BTO layer alleviate this problem so that a spontaneously polarized single-domain state can be formed. Even if the top surface is uncovered, the exposure to air is enough to attract ions that together with the La dopant will provide the conditions needed to cancel the depolarizing electric field (see supplementary material for further discussion).[13]

Note that a simple model in which the BTO is sandwiched between two shorted conducting layers would not fully account for the observed profile of oxygen displacements in the BTO film (see Fig. 3(b)). Shorted conducting layers would be expected to produce a uniform polarization in the film. In contrast, the observed oxygen displacements are significantly larger close to the surface than in bulk BTO, and decrease towards the interface with the LAO film. These observations imply that a substantial polarization gradient exists in the ferroelectric film.

Based on the observed polarization gradient in the BTO, we propose a model based on the uniform doping of the BTO film with La ions from the LTO layer. Associated with each La^{3+} dopant ion which replaces Ba^{2+} in the BTO is a Ti^{3+} ion that can ionize to a Ti^{4+} state, donating one electron to the conduction band. The presence of La within the BTO film leads to smoothly varying electric and polarization fields in the La-doped BTO.

We can account for the observed behavior with a model that includes the doping, electrostatic and free-energy considerations. We denote the electron-density $\rho(z) = (n_1 - n_2)e$. Here, e is the electron charge; n_1 and n_2 are the densities of La^{3+} ions and Ti^{3+} ions, respectively; $n_1 - n_2$ is the density of the Ti^{3+} ions ionized to Ti^{4+} ions; and z is the distance from the interface with the LAO film. The total number of La^{3+} ions per unit area is $N_1 = \int_0^L n_1 dz$, where $z = L$ corresponds to the sample surface. The value of N_1 is given in Table I.

We assume that the Fermi level in the film is far enough from the conduction band so that the density of free electrons is negligible at ambient temperature. This means that any electron excited from a Ti^{3+} ion is swept away to the gold contact. As seen below, this is consistent with the large electric field present in the film. Outside the BLTO film, Maxwell's displacement vector $\vec{D} = 0$. Inside the BLTO film, $\vec{D}$ satisfies $\vec{\nabla} \cdot \vec{D} = \rho$. So,

$$D(z) = \epsilon_0 \epsilon_\infty E(z) + P(z) = \int_0^z \rho dz = \sigma, \tag{1}$$

where $E(z)$ and $P(z)$ are the electric field and polarization at z, respectively. Here ϵ_∞ is the optical dielectric constant of the BTO film and ϵ_0 is the vacuum permittivity constant. Equation (1) yields

$$P(z) = \sigma - \epsilon_0 \epsilon_\infty E(z). \tag{2}$$

Both $P(z)$ and $E(z)$ are positive when they point in the positive direction (away from the substrate). Note that Eq. (1) satisfies the boundary condition $\vec{D} = 0$ at the interface with the LAO film ($z = 0$). The electric field and polarization should be such that the total free energy F is minimized, where

$$F = \int_0^L \left[\frac{\alpha}{2} P^2 + \frac{\beta}{4} P^4 + \frac{\gamma}{6} P^6 - EP + g \left(\frac{dP}{dz} \right)^2 \right] dz. \tag{3}$$

The room temperature values of α, β, and γ are given in Table I. g is estimated from reported gradient values.[15]

Now, using the Fermi distribution function, the charge density can be expressed in the following form:

$$\rho(z) = n_0 e \frac{exp[(\mathcal{E} + eV(z) - \mathcal{E}_F)/k_B T]}{1 + exp[(\mathcal{E} + eV(z) - \mathcal{E}_F)/k_B T]}. \tag{4}$$

Here, $n_0 = N_1/L$. The energy difference $\mathcal{E} - \mathcal{E}_F$ is determined at the interface with the Au electrode by the work functions of the electrode, the BTO film, and the La^{3+} and Ti^{3+} ion dopant energy levels. The associated potential difference $V(z)$ is

$$V(z) = -\int_z^L E dz. \tag{5}$$

Equations (1)–(5) can be solved self-consistently to obtain the charge density, the electric field, and the polarization as a function of position. We have solved the equations numerically using the parameters listed in Table I.

The polarization per unit volume obtained in this way is shown in Fig. 4(a) for energy differences $\mathcal{E} - \mathcal{E}_F$ between $10k_BT$ and $30k_BT$ in steps of $5k_BT$. The polarization is almost linear in z. Close to the surface when the energy difference is positive and large, the Ti^{3+} ions are fully ionized to Ti^{4+}. For large negative values, the polarization vanishes because the Ti^{3+} is no longer ionized to Ti^{4+}.

To compare the experimentally measured O1 displacements with the calculated polarization we use the Born effective charge. The Born effective charge of the apical oxygen of BTO is $-4.8e$.[20,21] This charge, and the experimentally measured oxygen displacements, yield the polarization shown by the red dots in Fig. 4(a). For $z < 1.5$ nm, the polarization is comparable to, or smaller than the spontaneous polarization in BTO. In this region the model calculated polarization and the polarization calculated using the Born effective charge are in good agreement. At $z > 1.5$ nm the two results tend to deviate suggesting that the Born effective charge decreases. This is expected because the electron-phonon interaction responsible for the large effective charge decreases when the displacements are large.

The size of the polarization per unit volume at the surface is larger than the spontaneous polarization in bulk BTO by a factor of 2. This is consistent with the very large oxygen displacement observed experimentally. The electric field profile is shown in Fig. 4(b). The presence of the large electric field on the side close to the surface is responsible for making the polarization larger than in bulk BTO. This large electric field is also responsible for the band bending and the change in the

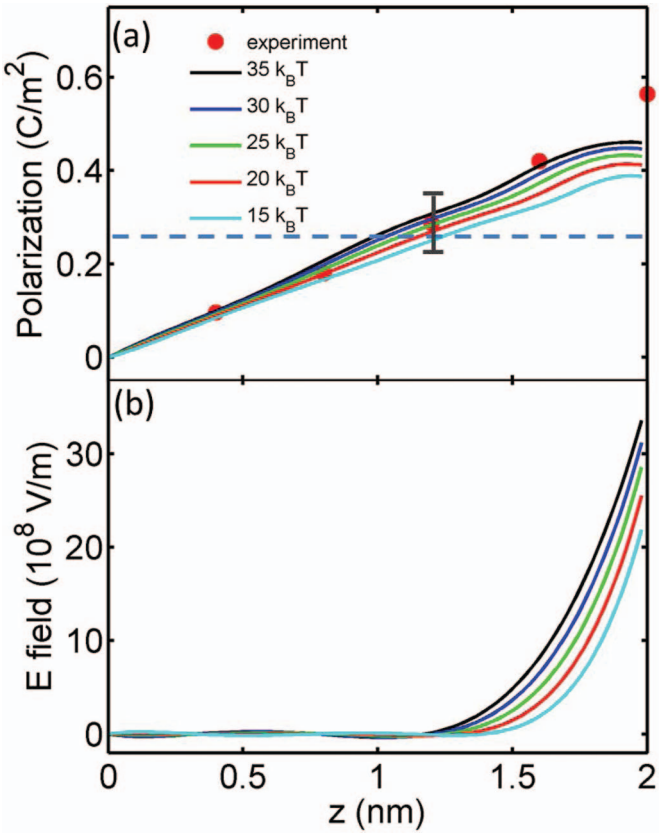

FIG. 4. (a) Calculated (lines) and experimental values of the polarization (circles) deduced by fitting displacements to the model described in the text. The error bar indicates the uncertainty in the experimental values. The dashed line indicates polarization of bulk BTO. (b) Electric field in La-doped BTO as a function of distance from the LAO interface. The theoretical curves are plotted as a function of the dopant energy relative to the Fermi level.

energy difference between the Ti^{3+} level and the Fermi energy. Notice that the polarization is stable in the direction towards the surface and hence, is not switchable.

Recent theoretical results on the $(LaO)^{+}$/BTO interface have also predicted a linear polarization in the BTO attributed to "charge leakage" due to the dipole formed by the charged $(LaO)^{+}$ layer with an enhanced polarization at the $(LaO)^{+}$/BTO interface.[22] In contrast, we observe a zero polarization at the nominal $(LaO)^{+}$/BTO interface with a polarization enhancement at the BTO surface which is in contact with a top metal electrode. The charge density and polarization profile observed in our BTO film is self-consistent with the presence of a uniform distribution of La in the BTO. While growth kinetics and thermodynamics may play a critical role in driving La/BTO intermixing, the uniform distribution of La, as determined by our analysis, suggests an electrostatic contribution to this effect.

In conclusion, we have presented a new approach to controlling and enhancing the spontaneous polarization profile of a BTO-based heterostructure. We find that ionic rearrangement results in strain reduction and minimizes the free energy of the system. The resultant structure eliminates the polarization discontinuity at the nominal BTO/LTO interface, leading to a 2-fold increase of the spontaneous polarization towards the surface of an ultra-thin single-domain BTO film. A theoretical model that takes into account the free energy and electrostatics of the system accounts quantitatively for these observations. The ability to experimentally observe the structural state of the system at the atomic scale, combined with a thorough understanding of the underlying mechanisms, is important for elucidating the role of interfaces in ferroelectric thin films and their optimization for various applications.

This work was supported by the U.S. Department of Energy, Office of Science, Basic Energy Sciences (Contract No. DE-FG02-06ER46273, PI: RC). Y.Y. acknowledges support from the Israel Science Foundation Grant No. 1005/11.

[1] P. Zubko, S. Gariglio, M. Gabay, P. Ghosez, and J.-M. Triscone, Annu. Rev. Condens. Mater. Phys. **2**, 141 (2011).
[2] J. W. Reiner, F. J. Walker, and C. H. Ahn, Science **323**, 1018 (2009).
[3] A. Ohtomo and H. Y. Hwang, Nature (London) **427**, 423 (2004).
[4] S. Thiel, G. Hammerl, A. Schmehl, C. W. Schneider, and J. Mannhart, Science **313**, 1942 (2006).
[5] S. A. Pauli, S. J. Leake, B. Delley, M. Björck, C. W. Schneider, C. M. Schlepütz, D. Martoccia, S. Paetel, J. Mannhart, and P. R. Willmott, Phys. Rev. Lett. **106**, 036101 (2011).
[6] M. L. Reinle-Schmitt, C. Cancellieri, D. Li, D. Fontaine, M. Medarde, E. Pomjakushina, C. W. Schneider, S. Gariglio, Ph. Ghosez, J.-M. Triscone, and P. R. Willmott, Nature Commun. **3**, 932 (2012).
[7] M. Dawber, C. Lichtensteiger, and J.-M. Triscone, Phase Transitions **81**, 623 (2008).
[8] S. Mathews, R. Ramesh, T. Venkatesan, and J. Benedetto, Science **276**, 238 (1997).
[9] P. R. Willmott, S. A. Pauli, R. Herger, C. M. Schlepütz, D. Martoccia, B. D. Patterson, B. Delley, R. Clarke, D. Kumah, C. Cionca, and Y. Yacoby, Phys. Rev. Lett. **99**, 155502 (2007).
[10] Y. Yacoby, M. Sowwan, E. A. Stern, J. O. Cross, D. Brewe, R. Pindak, J. Pitney, E. B. Dufresne, and R. Clarke, Nature Mater. **1**, 99 (2002).
[11] D. D. Fong, C. Cionca, Y. Yacoby, G. B. Stephenson, J. A. Eastman, P. H. Fuoss, S. K. Streiffer, C. Thompson, R. Clarke, R. Pindak, and E. A. Stern, Phys. Rev. B **71**, 144112 (2005).
[12] D. P. Kumah, S. Shusterman, Y. Paltiel, Y. Yacoby, and R. Clarke, Nat. Nanotechnol. **4**, 835 (2009).
[13] See supplementary material at http://dx.doi.org/10.1063/1.4849735 for additional details about the structural analysis.
[14] M. T. Buscaglia, V. Buscaglia, M. Viviani, P. Nanni, and M. Hanuskova, J. Eur. Ceram. Soc. **20**, 1997 (2000).
[15] Y. Yacoby, Y. Girshberg, E. A. Stern, and R. Clarke, Phys. Rev. B **74**, 104113 (2006).
[16] G. H. Kwei, A. C. Lawson, S. J. L. Billinge, and S.-W. Cheong, J. Phys. Chem. **97**, 2368 (1993).
[17] W. N. Lawless and R. C. DeVries, J. Appl. Phys. **35**, 2638 (1964).
[18] S. H. Wemple, M. Didomenico, Jr., and I. Camlibel, J. Phys. Chem. Solids **29**, 1797 (1968).
[19] Y. L. Wang, A. K. Tagantsev, D. Damjanovic, N. Setter, V. K. Yarmarkin, A. I. Sokolov, and I. A. Lukyanchuk, J. Appl. Phys. **101**, 104115 (2007).
[20] J. D. Axe, Phys. Rev. **157**, 429 (1967).
[21] Ph. Ghosez, J.-P. Michenaud, and X. Gonze, Phys. Rev. B **58**, 6224 (1998).
[22] Y. Wang, M. K. Niranjan, K. Janicka, J. P. Velev, M. Y. Zhuravlev, S. S. Jaswal, and E. Y. Tsymbal, Phys. Rev. B **82**, 094114 (2010).